ACS Catalysis

Research Article

pubs.acs.org/acscatalysis

Acid–Base Bifunctional Periodic Mesoporous Metal Phosphonates for Synergistically and Heterogeneously Catalyzing CO_2 Conversion

Tian Yi Ma and Shi Zhang Qiao*

School of Chemical Engineering, The University of Adelaide, Adelaide, SA 5005, Australia

Supporting Information

ABSTRACT: Integrating multiple functions into one host for improved catalytic performance is challenging and promising for both catalysis and material science. Herein a new acid–base bifunctional periodic mesoporous titanium phosphonate hybrid material is synthesized by a facile one-pot hydrothermal method, using alendronate sodium trihydrate as a coupling molecule. The new material possesses highly periodic mesopores with a large specific surface area of 540 $m^2\ g^{-1}$ and pore volume of 0.43 $cm^3\ g^{-1}$, favoring the smooth mass transport of reactants and products during the catalytic reaction. It also has an organic–inorganic hybrid framework with homogeneously incorporated phosphonate groups, in which a large number of accessible acidic P–OH and basic $-NH_2$ sites can, respectively, activate aziridine and CO_2, synergistically leading to the high conversion (>99%), yield (98%), and regioselectivity (98:2) for the CO_2 cycloaddition reaction. The catalytic activity is better than that of the scarcely reported heterogeneous catalysts for aziridine and CO_2 cycloaddition and even comparable to that of the state-of-the-art homogeneous ones. Moreover, being superior to the other catalysts, the metal phosphonate materials can be easily separated and reused repeatedly without activity loss, and no hazardous halogen ions, organic solvents, or cocatalysts are needed for the catalytic process. In comparison with previously reported multifunctional catalysts synthesized by complicated multistep fabrications, the facile one-pot preparation of mesoporous metal phosphonates with dual active sites makes it more practical for high-performance heterogeneous catalysis.

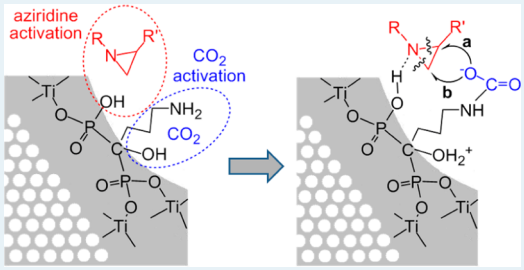

KEYWORDS: *phosphonate, bifunction, synergistic effect, heterogeneous catalysis, CO_2 conversion*

1. INTRODUCTION

Global warming is caused by the extensive emission of CO_2, and therefore, many efforts have been devoted to carbon capture and storage/sequestration (CCS).[1] Conversely, CO_2 can be used as a safe and cheap building block to produce useful organic compounds. For example, catalytic cycloaddition reaction of aziridine with CO_2 is one of the most efficient routes to transform CO_2 into oxazolidinones that are important intermediates in medicinal chemistry and synthetic chemistry, and many homogeneous catalysts such as alkali metal halides, iodines, α-amino acids, and ionic liquids have been studied for this reaction.[2] However, toxic organic solvents and cocatalysts, large CO_2 pressure, high reaction temperature, or long reaction time are often required to achieve satisfactory catalytic performance, and the toilsome product purification and catalyst separation/recycling are also the vital problems for homogeneous catalytic systems.[1b,2] Although heterogeneous catalysis may provide an alternative way to solve these problems, few reports involve heterogeneous catalysts (e.g., pyridinium halide functionalized chitosan,[3a] $ZrOCl_2$,[3b] and quaternary-ammonium-bromide-functionalized polyethylene glycol[3c]) for the cycloaddition reaction of CO_2 and aziridine, which all contain hazardous halogens to activate aziridines or stabilize the intermediates and suffer from gradually lost activity after recycling. Thus, it is very necessary to develop an environmentally and user-friendly heterogeneous catalyst for cycloaddition reaction of aziridines and CO_2 under relatively mild conditions.

Multifunctional catalysts with high activity, atom-economy, and step-saving properties are fabricated by combining multiple active sites into one matrix, in which antagonistic active sites, such as acid and base functions, are often involved.[4] Although the coexistence of acidic and basic sites has led to many diverse and flexible bifunctional catalysts, it still remains a great challenge for effectively suppressing their mutual deactivation and controlling chemically hostile active sites to smoothly accomplish their tasks. Locating these active sites on the separated domains of nanostructured supports is a useful strategy to fabricate acid–base bifunctional catalysts (e.g., encapsulating acidic and basic groups into different polymeric aggregates, and loading incompatible groups on core–shell or yolk–shell nanostructures).[5] Another efficient route is based on the multistep postmodification of organic–inorganic hybrid materials (e.g., mesoporous organosilicas),[4d,e,f] in which alternate grafting of acidic and basic groups by the means of H_2SO_4/NH_3 treatment, ion exchange, and organic reactions were usually employed. However, aforementioned strategies still have apparent disadvantages of complicated preparation

Received: August 3, 2014
Revised: September 14, 2014

   dx.doi.org/10.1021/cs501124d | ACS Catal. 2014, 4, 3847–3855

procedures associated with the construction of delicate nanostructures and complex postfunctionalization, as well as unsatisfactory catalytic activity; therefore, a simple method is urgently needed to prepare acid−base bifunctional catalysts.

Mesoporous metal phosphonates, as an important class of nonsiliceous hybrid materials, are nanocomposites of organic and inorganic components intimately mixed on a molecular level (though P−O−metal covalent bonds), combining the superiorities from both sides.[6] A large variety of phosphonic acids and their derivatives (e.g., salts or esters) with low cost and different functional groups can be used to construct metal phosphonates through sol−gel process and surface modification, rendering highly adjustable nanomorphologies (pores, spheres, wires, etc.) and chemical properties.[6a,b] Remarkably, the inherent acidity from dissociative P−OH groups (also called uncoordinated or defective P−OH) endows the metal phosphonate materials to be outstanding acid catalysts and ion exchangers.[7] However, up to now, only alkyl groups and tertiary amine species were introduced into the framework of mesoporous metal phosphonates, which displayed non or weakly alkaline property.[6,7] Consequently they all exhibited inferior affinity toward CO_2 adsorption and reactivity.[6b−g]

Herein periodic mesoporous titanium phosphonate materials are synthesized through a one-pot hydrothermal process by using amino-containing alendronate sodium trihydrate (AST, Scheme 1) as the coupling molecule (denoted as Ti-AST).

Scheme 1. Molecular Structures of Alendronate Sodium Trihydrate (AST) and Methylene Diphosphonic Acid (MDA)

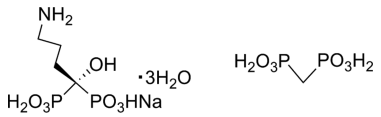

Both acidic P−OH and basic $-NH_2$ sites are simultaneously incorporated into the obtained organic−inorganic hybrid materials without further postmodification. Benefiting from the synergistic effect of P−OH and $-NH_2$ groups that can respectively activate aziridine and CO_2, Ti-AST is highly active for heterogeneously catalyzing cycloaddition reaction between aziridine and CO_2 in a solvent-free system to yield oxazolidinones without introducing any cocatalysts or halogen species. Moreover, the used catalysts can be easily recovered by filtration while retaining the original high activity.

2. EXPERIMENTAL SECTION

2.1. Materials. Titanium tetrachloride ($TiCl_4$), alendronate sodium trihydrate (AST), methylene diphosphonic acid (MDA), and Brij 56 ($C_{16}H_{33}(OCH_2CH_2)_{10}OH$) were obtained from Sigma-Aldrich Chemical Co. The structures of AST and MDA are shown in Scheme 1. All chemicals were used as received without further purification.

2.2. Synthesis of Periodic Mesoporous Titanium Phosphonates (Ti-AST). In a typical synthesis procedure, 1.2 g of Brij 56 and 0.005 mol of AST were added into a mixed solution of 15 mL of deionized water and 45 mL of ethanol under vigorous stirring, followed by dropwise addition of $TiCl_4$ (P/Ti molar ratio: 5/3) very slowly. The pH value of the mixture was adjusted by ammonia and hydrochloric acid and kept at ca. 4.0 through the entire preparation process. A homogeneous mixture was obtained after 2 h of stirring, and the mixture was then sealed in one Teflon-lined autoclave and aged statically at 120 °C under autogenous pressure for 48 h. The obtained gels were dried at 110 °C and transferred carefully to a Soxhlet extractor to remove the surfactant by ethanol extraction for 24 h. The final product was denoted as Ti-AST.

2.3. Synthesis of the Control Groups. For the purpose of comparison, mesoporous titanium phosphonates with insufficient acidic P−OH groups were prepared under the same conditions to the synthesis of Ti-AST by using AST as the coupling molecule, but at a decreased P/Ti molar ratio of 1/1, it was denoted as Ti-AST′. Similar procedures were carried out to synthesize mesoporous titanium phosphonates with no basic groups using the coupling molecule MDA at P/Ti molar ratio of 5/3, and the product was denoted as Ti-MDA. As the nonporous counterpart of mesoporous Ti-AST, bulk titanium phosphonates denoted as Bulk-Ti-AST were prepared by using the same method to the synthesis of Ti-AST, but without addition of Brij 56 surfactant as the mesopore-forming agent. The textural properties of the synthesized materials were summarized in Table S1 in Supporting Information.

2.4. Cycloaddition Reaction between Aziridines and CO_2. Aziridine (1 mmol) and mesoporous titanium phosphonate catalysts were added into a stainless autoclave reactor with a magnetic stirrer. ***Caution!*** *Aziridines are irritants to mucosal surfaces including eyes, nose, respiratory tract and skin, and are possibly carcinogenic to humans. Direct contact must be avoided! Researchers handling aziridines are required to wear appropriate personal protective equipment.* CO_2 was introduced into the autoclave, and the system was adjusted to the desired pressure and temperature. The mixture was stirred continuously under this condition for various reaction periods. After the reaction, the reactor was cooled in cold water, and extra CO_2 was vented slowly. The conversion of the catalytic system was obtained from gas chromatography, and the yield was calculated using biphenyl as an internal standard. The residue was purified over a silica gel by column chromatography using petroleum ether/ethyl acetate (10/1 to 1/1) as the eluant to afford products. The structural data of the oxazolidinone products were shown in Supporting Information. In the catalyst recycling process, the catalyst was first recovered from the reaction mixture by filtration, washed with dichloromethane, and dried overnight at 80 °C in vacuum. Then the recovered catalyst was reused for CO_2 conversion.

2.5. Physicochemical Characterization. Transmission electron microscopy (TEM) analysis was carried out on a JEM-2100F microscope. X-ray diffraction (XRD) patterns were recorded on a Rigaku D/max 2500v/pc diffractometer. The chemical compositions of the samples were analyzed by inductively coupled plasma (ICP) emission spectroscopy on a Plasma1000 spectrometer, and C, N, and H contents were analyzed on a WS-CHN800 elemental analyzer. Thermogravimetric analysis (TG) was performed using a Netzsch STA409 instrument at a heating rate of 5 °C min^{-1} using α-Al_2O_3 as the reference. Fourier transform infrared (FT-IR) spectra were measured on a Bruker VECTOR 22 spectrometer with KBr pellet technique, and the ranges of spectrograms were 400 to 4000 cm^{-1}. Pyridine-adsorbed IR spectra were performed with a Nicolet Nexus 470 model FT-IR spectrometer. Samples were first activated in vacuum at 200 °C for 2 h, followed by pyridine adsorption for 30 min at room temperature. Then the temperature was raised and held at the desired value for 1 h

dx.doi.org/10.1021/cs501124d | ACS Catal. 2014, 4, 3847−3855

before recording the spectrum. X-ray photoelectron spectra (XPS) were determined using a Thermo Escalab 250 spectrometer equipped with a monochromatic Al Kα X-ray source. Solid-state ^{31}P magic angle spinning nuclear magnetic resonance (^{31}P MAS NMR) measurement was performed on a Varian Unity plus-400 spectrometer at spinning rate of 12 kHz and resonance frequency of 161.9 MHz with recycle time of 5 s. N_2 adsorption isotherms were collected on a Tristar II, Micromeritics adsorption analyzer at −196 °C. The samples were degassed at 200 °C in vacuum for 12 h prior to the analysis. Pore-size distributions were calculated using the adsorption branch of isotherms by the Barrett−Joyner−Halenda (BJH) method; surface areas were obtained by the Brunauer−Emmett−Teller (BET) method using adsorption data at a relative pressure range of P/P_0 = 0.05−0.30; and total pore volumes were estimated from the volume adsorbed at a relative pressure (P/P_0) of 0.994. The CO_2 adsorption isotherms of the samples were measured using a Micromeritics ASAP 2020 at 0, 45, and 90 °C. Each sample was outgassed for 12 h at 200 °C to remove the guest molecules from the pores and then cooled to room temperature, followed by the introduction of CO_2 into the system. The acid content was determined from the titration curve.[7] Specifically, 50 mg of the solid sample was immersed in 10 wt % sodium chloride aqueous solution for 24 h. The solution was titrated with 0.05 mol L^{-1} NaOH to produce the titration curve. A differential titration curve was drawn to determine the acid content at the inflection. NH_3 temperature-programmed desorption (NH_3-TPD) experiments were carried out on a Micromeritics Autochem 2910. Approximately 0.2 g of sample was heated to 200 °C under the flow of pure He gas with a rate of 10 °C min^{-1} and kept at this temperature for 1 h. After the sample was cooled to room temperature for NH_3 adsorption with 10% NH_3/Ar, the gas was switched to pure He gas until the baseline was stable. Then the NH_3-TPD curve was measured at a rate of 10 °C min^{-1}. CO_2-TPD experiments were performed similarly by replacing NH_3/Ar with high-purity CO_2.

3. RESULTS AND DISCUSSION

3.1. TEXTURAL AND SPECTROSCOPIC PROPERTIES.

The synthesis of periodic mesoporous titanium phosphonates involved the condensation of $TiCl_4$ and AST in the presence of oligomeric template Brij 56 in water/ethanol mixed solvent, the hydrothermal aging process, and the removal of surfactant species through ethanol extraction (see details in Experimental Section). The hexagonal arrangement of mesopores in Ti-AST can be clearly seen from the TEM image (Figure 1a). Typical one-dimensional channels are observed from the side view of the solid (Figure 1b). The uniform dispersion of Ti, P, and N elements in Ti-AST verifies a homogeneous distribution of organic groups inside the hybrid material framework (energy dispersive X-ray spectroscopy (EDS) elemental mapping image, Figures 1c−e). The low-angle XRD pattern (Figure 1f) of Ti-AST shows a main peak located at 2θ = 2.33° corresponding to the diffraction of (100) plane (d_{100} = 3.7 nm) and two small peaks at 2θ = 3.89 and 4.45° can be attributed to the diffractions of (110) and (200) planes, which displays a typical hexagonal mesophase (*p6mm*) consistent to TEM images. The unit cell parameter (a) was calculated to be 4.3 nm. The wide-angle XRD pattern indicates the amorphous pore wall of Ti-AST with no crystalline TiO_2 phase detected (Figure 1f inset), implying the extensive formation of amorphous titanium phosphonate skeleton. The N_2 adsorption isotherm of Ti-AST is of type IV with no visible hysteresis loop, showing reversible capillary condensation−evaporation in mesopores (Figure 1g), which is typical for ordered organic−inorganic nanocomposites (OOINs) with accessible mesostructures.[8] Correspondingly, one narrow peak centered at 2.4 nm is observed in the pore-size distribution curve (Figure 1g inset), indicating the uniform pore size of Ti-AST. Besides, Ti-AST possesses the high surface area and large pore volume of 540 m^2 g^{-1} and 0.43 cm^3 g^{-1}, respectively, indicating the highly porous nature of Ti-AST.

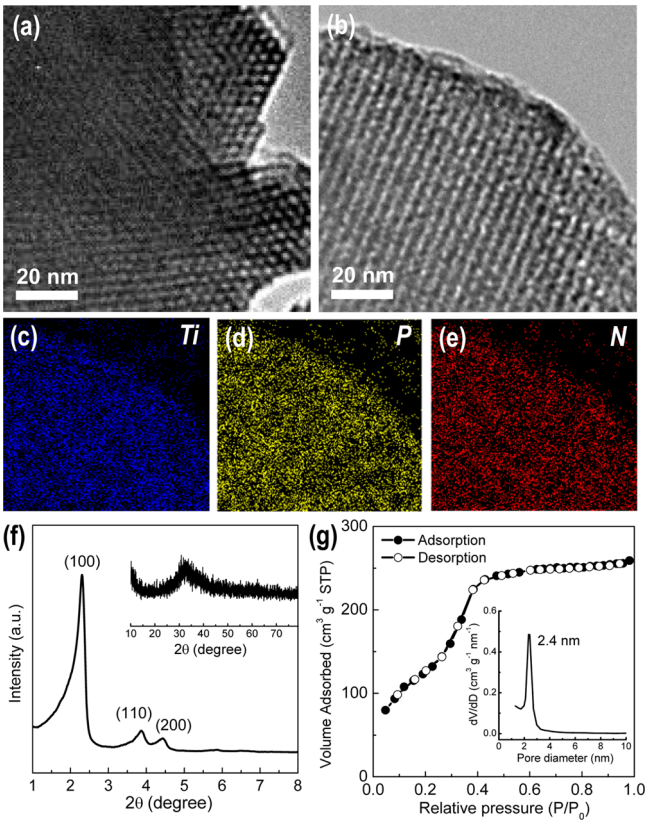

Figure 1. (a, b) TEM, (c−e) EDS elemental mapping images, (f) low-angle and (inset of f) wide-angle XRD patterns, (g) N_2 adsorption isotherm and (inset of g) the corresponding pore size distribution curve of Ti-AST.

The homogeneously organic−inorganic hybrid framework of Ti-AST was confirmed by FT-IR, MAS NMR, and XPS. As shown in the FT-IR spectrum of Ti-AST (Figure 2a), the strong band at 1035 cm^{-1} is due to P−O−Ti stretching vibrations evidencing the formation of titanium phosphonate framework, while the band at 960 cm^{-1} is assigned to uncoordinated P−OH (acidic P−OH) stretching vibrations.[7] The basic amino groups are revealed by the sharp peak at around 3448 cm^{-1} assigned to the stretching vibrations of $-NH_2$, and the peaks at 1650 and 615 cm^{-1}, which are characteristic of the bending vibrations of $-NH_2$ groups.[9] Additionally, the small band at 1370 cm^{-1} related to the phosphoryl (P═O) frequency, the band at 1148 cm^{-1} of C−O stretching vibrations, and weak bands around 2900−2980 cm^{-1} due to the C−H stretching modes in $-(CH_2)_3-$ groups all confirm that the organic motifs in AST coupling molecule are well-preserved in Ti-AST.

The solid-state ^{31}P MAS NMR spectrum of Ti-AST shows one broad signal at 14.7 ppm (Figure 2b) and another shoulder

dx.doi.org/10.1021/cs501124d | ACS Catal. 2014, 4, 3847−3855

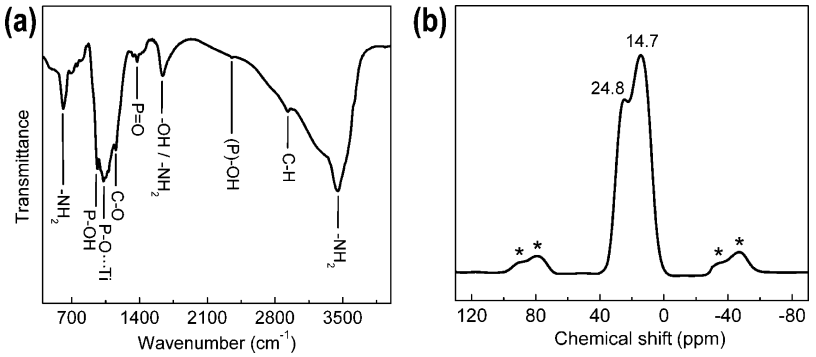

Figure 2. (a) FT-IR and (b) solid-state ^{31}P MAS NMR spectra of Ti-AST.

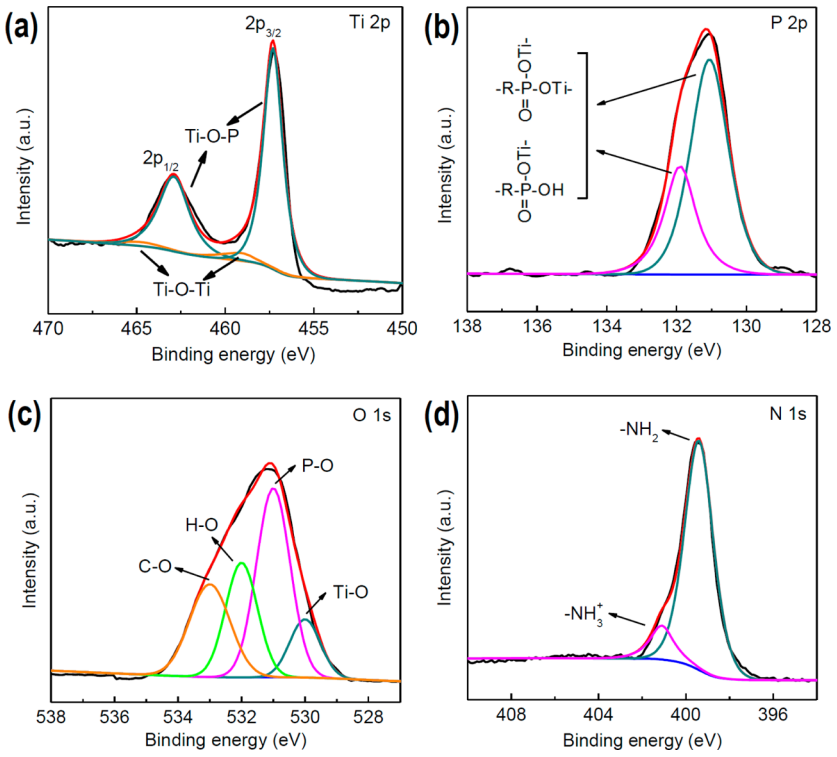

Figure 3. High-resolution XPS spectra of the Ti 2p, P 2p, O 1s, and N 1s core levels in Ti-AST.

peak at 24.8 ppm, which are both in the typical region of organo-phosphonates.[6,7a,b] These two signals can be assigned to phosphonic acid fully and partially coordinated by titanium in the forms of −R−P(═O)(−OTi−)$_2$ and −R−P(═O)-(−OH)(−OTi−), respectively (R: organic bridging groups in phosphonic acids), of which the dissociative P−OH groups (acidic groups) are originated from the latter.

The XPS spectrum of Ti 2p in Ti-AST is best deconvoluted with the assumption of four species, in which two peaks at 457.3 and 462.9 eV are related to the Ti species with Ti−O−P bonding mode,[6] and another two peaks at 459.0 and 464.8 eV are attributed to the Ti species with Ti−O−Ti bonding mode (Figure 3a).[10] Notably, the Ti content in Ti−O−Ti clusters is negligible in comparison to that in Ti−O−P clusters, indicating Ti atoms are extensively linked to AST coupling molecules through Ti−O−P bonds instead of forming large TiO_2 aggregates, in accordance with the wide-angle XRD pattern. An unsymmetrical signal is observed for the P 2p binding energy in the range of 130−133 eV (Figure 3b), which is characteristic of P^{5+} in phosphonate groups.[7a,b] The unsymmetrical shape is originated from the P displaying different bonding modes of −R−P(═O)(−OTi−)$_2$ and −R−P(═O)(−OH)(−OTi−), consistent with FT-IR and ^{31}P MAS NMR results, which corroborates the presence of numerous acidic P−OH groups. The broad O 1s spectrum can be best deconvoluted into four species, situated at around 530.0, 530.9, 532.1, and 533.2 eV, which are ascribed to oxygen contributed from Ti−O, P−O, H−O, and C−O, respectively (Figure 3c). The main peak in the N 1s spectrum at 399.5 eV is due to the amino groups (−NH_2) in AST (Figure 3d), while another shoulder peak at 401.1 eV implies a small portion of protonated amino groups (−NH_3^+).[10]

The thermal stability of Ti-AST was investigated by TG analysis (Figure S1). The weight loss from room temperature to 140 °C is attributed to the evaporation of the physically adsorbed water and gases, and the continuous weight loss of 22.1% from 235 to 850 °C is due to the decomposition of phosphonate species and coke combustion, suggesting that Ti-AST is thermally stable to ∼235 °C. A P/Ti molar ratio of 1.65 (19.21 wt % P, 17.92 wt % Ti) in the resultant materials is

dx.doi.org/10.1021/cs501124d | ACS Catal. 2014, 4, 3847−3855

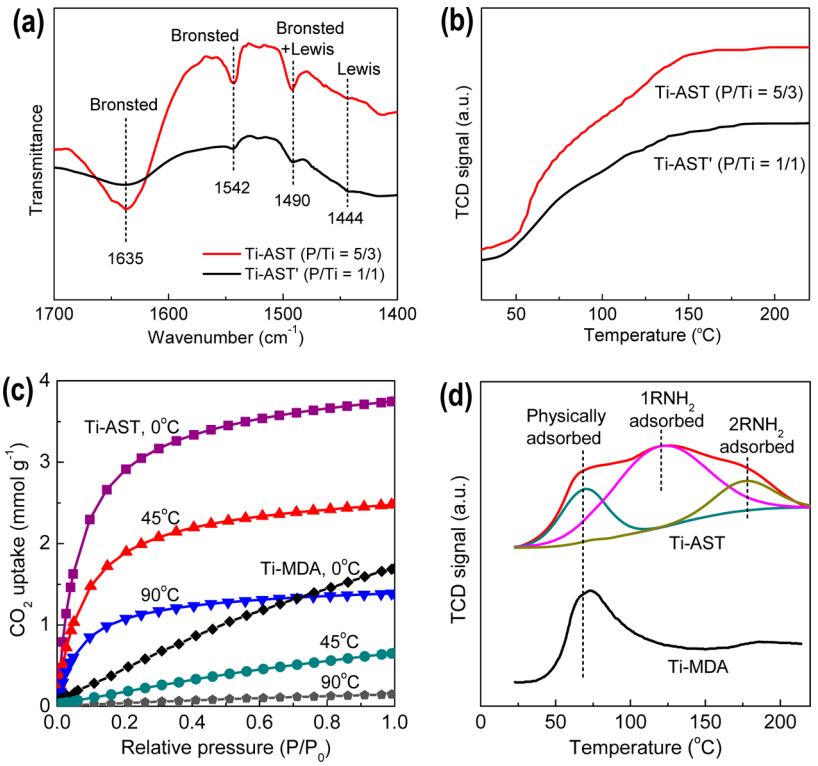

Figure 4. (a) Pyridine-adsorbed IR spectra and (b) NH_3-TPD curves of Ti-AST and Ti-AST′ synthesized at different P/Ti molar ratios. (c) CO_2 adsorption isotherms and (d) CO_2-TPD curves of Ti-AST and Ti-MDA synthesized from different phosphonic acids.

confirmed by the ICP emission spectroscopy, revealing a substantial high-content incorporation of phosphonate groups into Ti-AST. Therefore, on the basis of EDS, FT-IR, MAS NMR, XPS, and TG measurements, no phase separation occurred during the preparation of Ti-AST, and the AST coupling molecules are dispersed homogeneously within the organic−inorganic hybrid titanium phosphonate framework, affording abundant acidic P−OH and basic $-NH_2$ sites and moderate thermal stability.

3.2. ACID−BASE BIFUNCTIONAL SURFACE. The acidity of Ti-AST was examined by pyridine-adsorbed IR spectra, NH_3-TPD, and titration curves. The pyridine-adsorbed IR spectrum of Ti-AST shows two sharp peaks at 1635 and 1542 cm^{-1} (Figure 4a), typical bands of pyridinium ions formed by the interaction between pyridine and Brønsted acidic sites (P−OH), which suggests that P−OH groups of Ti-AST can act as accessible acidic sites and interact with N-containing substrates,[11] being potentially useful for catalytic reactions associated with aziridines. The very weak peak at 1444 cm^{-1} is attributed to the adsorbed pyridine at Lewis acidic sites, while the band at 1490 cm^{-1} is contributed by both Brønsted and Lewis acidic sites.[12] When the feeding P/Ti molar ratio in the preparation was decreased to 1/1 (denoted as Ti-AST′, see synthesis details in Experimental Section), the bands at 1635, 1542, and 1490 cm^{-1} are dramatically weakened, indicating the substantial loss of Brønsted acidic sites. In Ti-AST′, Ti species with increased content in comparison to that in Ti-AST (P/Ti = 5/3) can coordinate with more P−OH groups, consequently reducing the Brønsted acid content.[7] This phenomenon further corroborates that the inherent acidity of titanium phosphonates is originated from dissociative P−OH groups.

The NH_3-TPD measurement was performed from room temperature to ∼220 °C, considering that no higher temperature is required in the following cycloaddition reaction. The NH_3 desorption volume of Ti-AST exceeds that of Ti-AST′ (Figure 4b), revealing more moderate/weak acidic sites existing in Ti-AST than those in Ti-AST′, in accordance with the pyridine-adsorbed IR result. The acid content of the samples was also determined from the titration curve (see details in Experimental Section), showing 4.82 and 2.55 mmol (H^+) g^{-1} (catalyst) for Ti-AST and Ti-AST′, respectively. The high acid content of Ti-AST, originated from P−OH groups, is comparable to that of previously reported hybrid metal phosphonate (3.9−5.9 mmol g^{-1})[7a,b] and inorganic metal phosphate (1.7−3.4 mmol g^{-1})[7c,d] acid catalysts.

The affinity of Ti-AST toward CO_2 was measured by CO_2 adsorption and CO_2-TPD. The CO_2 adsorption isotherms of Ti-AST significantly depart from linearity with a steep rise at the initial pressure (Figure 4c), which is the typical profile for chemical adsorption.[13] This is because the chemical adsorption requires lower activation energy than that of the physical adsorption, facilitating CO_2 adsorption at low relative pressure via much stronger interaction between CO_2 molecules and $-NH_2$ groups of Ti-AST. The highest CO_2 uptake of Ti-AST at 0 °C is 3.75 mmol g^{-1}, much higher than that of the previously reported porous metal phosphonates without $-NH_2$, which failed in CO_2 chemical adsorption and conversion,[6b−g] and comparable to that of some $-NH_2$-functionalized metal−organic frameworks (MOFs) and porous silicas.[14] On the contrary, a nearly linear relationship between adsorption capacity and relative pressure, characteristic for physical adsorption,[13] is observed for Ti-MDA, which is prepared by methylene diphosphonic acid without $-NH_2$ groups (MDA, Scheme 1, see synthesis details in Experimental Section). The CO_2 uptake of Ti-MDA at 0 °C is 1.68 mmol g^{-1}, much lower than that of Ti-AST, despite the higher specific surface area of

dx.doi.org/10.1021/cs501124d | ACS Catal. 2014, 4, 3847−3855

Table 1. Catalytic Activity of Mesoporous Titanium Phosphonate Materials for Cycloaddition Reaction between CO_2 and Aziridine

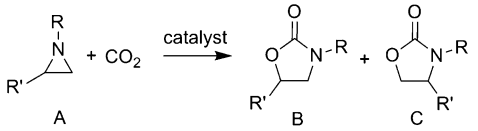

A B C

entry	catalyst[a]	substrate (R, R′)[b]	temperature (°C)	pressure (MPa)	time (min)	conversion (%)[c]	yield (%)[d]	regioselectivity[e]
1	none	Et, Ph	120	3.5	600	37	27	95:5
2	Ti-MDA	Et, Ph	80	3.0	30	55	48	96:4
3	Ti-AST′	Et, Ph	80	3.0	30	67	58	95:5
4	bulk-Ti-AST	Et, Ph	80	3.0	30	60	53	97:3
5	AST	Et, Ph	80	3.0	30	>99	98	98:2
6		Et, Ph	80	3.0	30	>99	98	98:2
7		Et, Ph	60	3.0	30	53	48	96:4
8		Et, Ph	120	3.0	30	>99	96	96:4
9		Et, Ph	80	7.0	30	>99	98	98:2
10	Ti-AST	*n*-Pr, Ph	80	3.0	30	97	95	97:3
11		*n*-Bu, Ph	80	3.0	180	94	92	98:2
12		Et, *p*-Cl-Ph	80	3.0	180	>99	95	97:3
13		Et, *p*-Me-Ph	80	3.0	180	95	92	97:3
14		*c*-Hex, Ph	100	3.0	2400	>99	90	99:1
15		*c*-Hex, *p*-Me-Ph	100	3.0	2400	99	94	>99:1
16		*c*-Hex, *p*-Cl-Ph	100	3.0	2400	99	96	99:1

[a]Reaction conditions: 1.0 mmol of **A**, 1.0 mol % of catalyst. [b]Et: ethyl, Ph: phenyl, *n*-Pr: *normal*-propyl, *n*-Bu: *normal*-butyl, *p*-Cl-Ph: *para*-chlorophenyl, *p*-Me-Ph: *para*-tolyl, *c*-Hex: cyclohexyl. [c]The conversion was calculated based on aziridines. [d]The total yield of **B** and **C**. [e]Molar ratio of **B** to **C**.

Ti-MDA (627 $m^2\ g^{-1}$) than that of Ti-AST (540 $m^2\ g^{-1}$, Table S1). The inferior adsorption capacity is the result of the weak physical interaction between Ti-MDA and CO_2 molecules. Moreover, a considerable chemical uptake of 1.35 mmol g^{-1} on Ti-AST is retained even at 90 °C, whereas the physical uptake on Ti-MDA at 90 °C is very low (0.14 mmol g^{-1}), declaring the superiority of chemical adsorption (i.e., strong uptake at relatively high temperatures).[13]

In the CO_2-TPD profiles (Figure 4d), Ti-MDA shows one peak centered at 69 °C, due to the desorption of physically adsorbed CO_2. Besides this signal, Ti-AST exhibits two new peaks centered at 120 and 176 °C. Specifically, the smaller peak at 176 °C is originated from the desorption of chemically adsorbed CO_2, in which two $-NH_2$ are involved for one CO_2 molecule capture ($-NH_2/CO_2 = 2$):[15]

$$CO_2 + 2RNH_2 \rightarrow RNHCOO^- + RNH_3^+ \quad (1)$$

Noticeably, the dominating peak at 120 °C is attributed to carbamate formation with assistance of hydroxyl groups ($-OH$) in the AST molecule:[15b,16]

$$CO_2 + R'OH + RNH_2 \rightarrow R'OH_2^+ + RNHCOO^- \quad (2)$$

The reaction 2 not only increases the utilization efficiency of $-NH_2$ ($-NH_2/CO_2 = 1$ vs $-NH_2/CO_2 = 2$ in reaction 1), but also generates intermediate carbamates with lower thermal stability,[15,16] which facilitates the CO_2 desorption and promotes the next step of cycloaddition reaction.

3.3. CO_2 CHEMICAL CONVERSION. The acid−base bifunctional feature endows Ti-AST with great potential in catalyzing cycloaddition reaction between aziridine and CO_2, without using any solvents, cocatalysts, or other additives. 1-Ethyl-2-phenylaziridine is investigated as a representative substrate under an optimized reaction condition—that is a 30 min reaction at 80 °C and 3.0 MPa (Table 1). Ti-AST affords a high conversion of >99% and a high yield of 98% for B + C, with a regioselectivity of 98/2 for B/C (entry 6), which are much higher than those without catalysts (entry 1, conversion: 37%, yield: 27%, regioselectivity: 95:5), those of Ti-MDA with no basic sites (entry 2, conversion: 55%, yield: 48%, regioselectivity: 96:4) and Ti-AST′ with insufficient acidic sites (entry 3, conversion: 67%, yield: 58%, regioselectivity: 95:5) under the same conditions, demonstrating the significant importance of acid−base bifunctionality of Ti-AST. Remarkably, the excellent activity and selectivity of the heterogeneous Ti-AST catalyst are not only comparable to those of the homogeneous AST coupling molecule (entry 5, conversion: >99%, yield: 98%, regioselectivity: 98:2) and the state-of-the-art homogeneous ones[2] but also superior to the reported heterogeneous catalysts[3] in terms of higher activity, milder working conditions (lower temperature and pressure), and environmentally friendly pathway (no halogens and organic solvents). Note that the present catalytic system shows high selectivity toward the main products of B and C, with very low amounts of the homopolymerization oligomers of aziridines and the copolymerization oligomers of aziridines/CO_2 as the byproducts (e.g., 1,4-diethyl-2,3-diphenylpiperazine and 1,4-diethyl-2,5-diphenylpiperazine).

Further experiments indicate that the reaction temperature is critical in the present catalysis system. The decomposition of intermediate carbamates to release chemically adsorbed CO_2 for cycloaddition process is directly relevant to the reaction temperature. When the reaction temperature is lowered to 60 °C, the catalytic performance drops dramatically (entry 7, conversion: 53%, yield: 48%) in comparison to that at 80 °C (entry 6), because it is difficult for the activated (chemically adsorbed) CO_2 molecules to be released from the catalyst surface at low temperatures (as evidenced by CO_2-TPD, Figure 4d). Although physically adsorbed CO_2 also exists on the pore

dx.doi.org/10.1021/cs501124d | ACS Catal. 2014, 4, 3847−3855

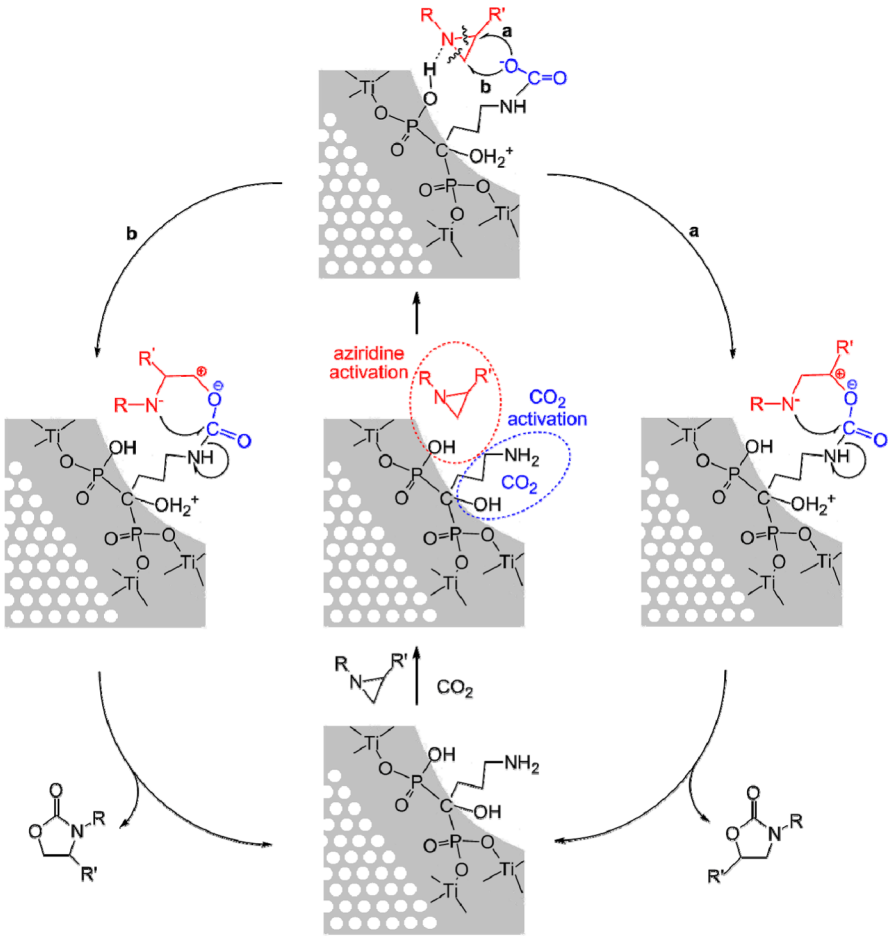

Figure 5. Proposed reaction mechanism initiated on bifunctional Ti-AST.

surface of Ti-AST at low temperatures, these molecules can hardly react with aziridines due to their unactivated fashion. Further increasing the temperature to 120 °C does not improve the activity apparently (entry 8), suggesting that the reaction temperature of 80 °C is appropriate to initiate the reaction. Moreover, the high conversion (>99%) and yield (98%) with excellent regioselectivity (98/2) can be achieved in a wide range of CO_2 pressure of 3.0−7.0 MPa (entries 6, 9).

Various oxazolidinones can be synthesized through cycloaddition reaction between CO_2 and different organic-group-substituted aziridines catalyzed by Ti-AST (entries 10−16). The high conversion of 94% to >99% and high yield of 90% to 96% with good regioselectivity of 97/3 to >99/1 can be obtained with changing either the alkyl substituent at the nitrogen atom or the substituent on phenyl, confirming the versatility of this bifunctional Ti-AST catalyst. When larger substituents, such as butyl (entry 11), cyclohexyl (entries 14−16), chlorophenyl (entries 12, 16), and tolyl (entries 13, 15), are introduced in the reactants, relatively higher temperature (100 °C for entries 14−16) and longer reaction time (180 min for entries 11−13, 2400 min for entries 14−16) were required to obtain the satisfactory results, which is due to the increased steric hindrance caused by the aziridines containing large substituents, and their higher diffusion resistance and slower mass transport rate within the porous channels of Ti-AST.

Another advantage of the synthesized mesoporous phosphonate materials is their excellent recyclability, which benefits from the heterogeneously catalytic process under solvent-free conditions without cocatalysts. The Ti-AST catalyst can be easily recovered from the reaction mixture by filtration and washing and can be reused for the next run. As shown in Table S2, no substantial drop of the catalytic activity in terms of conversion, yield and regioselectivity is found after 10 cycles, much better than that of previously reported cycloaddition catalysts.[2,3] Also, the mesoporous structure of Ti-AST after it is used for 10 cycles is well-preserved, which is confirmed by the N_2 adsorption isotherm (Figure S2a, only 5% deterioration of the specific surface area), the low-angle XRD pattern and TEM image (Figure S2b, similar hexagonal mesoporous structure before and after 10 cycles). On the contrary, although the coupling molecule AST, directly used as a homogeneous catalyst, can show the similar catalytic activity to that of Ti-AST, it suffers from toilsome product purification and difficult catalyst separation/recycling, making it unsuitable for practical applications.

The outstanding catalytic activity of Ti-AST is originated from both the acid−base bifunctional surface property and the periodic mesoporous structure. On the basis of the aforementioned material characterization and catalytic activity evaluation, a possible mechanism for the mesoporous metal phosphonate-catalyzed cycloaddition reaction is illustrated in Figure 5, featuring a synergistic effect of the acid−base bifunctional sites in Ti-AST. Initially, the Brønsted acidic sites (P−OH) on the pore wall of Ti-AST interact with the nitrogen of aziridines (as evidenced by pyridine-adsorbed IR and NH_3-TPD), resulting in the activation of aziridine, which is quite

dx.doi.org/10.1021/cs501124d | ACS Catal. 2014, 4, 3847−3855

different from previous cycloaddition catalysts that require halogens to activate aziridines and stabilize intermediates.[2,3] In the meantime, CO_2 molecules are activated by $-NH_2$ and −OH groups (reaction 2), forming carbamate species (as proven by CO_2 adsorption and CO_2-TPD),[15,16] which further nucleophilically attack the aziridine ring activated by P−OH. Due to the conjugation effect between carbonium ions and the neighboring benzene, $R'CH^+$ (R′ representing aromatic groups) is more stable than $R'CHCH_2^+$, thus the pathway **a** (Figure 5) is preferred via a ring-opening reaction occurred at the sterically hindered side of the aziridine ring. This is also consistent to the fact that the bond dissociation energy of R′CH−NR is lower than that of $R'CHCH_2$−NR in aziridines.[17] Thus, the regioselectivity in this ring-opening reaction results in the highly regioselective formation of oxazolidinones. Finally, the intramolecular cyclization via nucleophilic attack leads to the oxazolidinone products and the complete decomposition of carbamates that releases $-NH_2$ and regenerates the Ti-AST catalyst. This efficient reaction cycle can be only achieved in the presence of both abundant acidic and basic sites on Ti-AST. On the contrary, for Ti-MDA without $-NH_2$ (entry 2), CO_2 molecules physically adsorbed on the pore surface can not be activated to form carbamate, which fail to nucleophilically attack the aziridine; while for Ti-AST′ with insufficient P−OH (entry 3), the majority of aziridine molecules remain inert without fully activation by P−OH, resulting in the low catalytic activity.

The function of porous structure was demonstrated by comparing the activity of mesoporous Ti-AST with that of Bulk-Ti-AST, a nonporous titanium phosphonate with acid−base bifunctional surface and P/Ti molar ratio of 5/3 synthesized in the absence of Brij 56 templates (see details in Experimental Section). Unsurprisingly, Bulk-Ti-AST exhibits inferior activity for CO_2 cycloaddition reaction with a low conversion of 60% and yield of 53% (entry 4). If the total yields for the main products (B + C) were further normalized by the specific surface area, the value of Bulk-Ti-AST (0.015 g m^{-2}) is higher than that of Ti-AST (0.002 g m^{-2}), which implies that the catalytic activity of the metal phosphonates is not proportional to the surface area. Thus, the higher catalytic activity of Ti-AST than its nonporous counterpart should be preferably attributed to the enhanced mass transport of reactants and products within the well-developed pores that promotes the reaction kinetics, rather than simply due to the large surface area.[18] Therefore, being fundamentally different from previous reported catalysts, mesoporous bifunctional Ti-AST is capable of catalyzing cycloaddition reaction between CO_2 and aziridine under mild conditions without introducing halogens, organic solvents, and cocatalysts, featuring a highly efficient and environmentally benign conversion process.

4. CONCLUSION

In summary, periodic mesoporous titanium phosphonate materials, containing bifunctional acidic (P−OH) and basic ($-NH_2$) groups, were prepared by a facile surfactant-assisted hydrothermal process. The acid−base bifunctional Ti-AST exhibits outstanding activity and selectivity in catalyzing the cycloaddition reaction between aziridine and CO_2, in which the P−OH and $-NH_2$ groups, respectively, activate aziridine rings and CO_2 molecules, while the periodic mesoporous structure with large surface area benefits the smooth transport of reactants and products. The performance of Ti-AST is much better than that of its nonporous counterpart, titanium phosphonates without basic sites or with insufficient acidic sites, and other heterogeneous catalysts reported to date, and also comparable to that of the highly active homogeneous ones. This new class of porous metal phosphonate-based bifunctional materials is expected to be useful in cascade reactions, epoxide and CO_2 cycloaddition, and other reactions that require multiple catalytic active sites.

■ ASSOCIATED CONTENT

Supporting Information

Physicochemical property summary of catalysts, recyclability test, N_2 adsorption, XRD and TEM after recycle, TG curve of Ti-AST, and spectroscopic data of oxazolidinones. This material is available free of charge via the Internet at http://pubs.acs.org.

■ AUTHOR INFORMATION

Corresponding Author

*E-mail: s.qiao@adelaide.edu.au. Fax: +61-8-83134373. Tel.: +61-8-83136443.

Notes

The authors declare no competing financial interest.

■ ACKNOWLEDGMENTS

This work is financially supported by the Australian Research Council (ARC) through the Discovery Project programs (DP140104062 and DP130104459).

■ REFERENCES

(1) (a) Lescot, C.; Nielsen, D. U.; Makarov, I. S.; Lindhardt, A. T.; Daasbjerg, K.; Skrdstrup, T. *J. Am. Chem. Soc.* **2014**, *136*, 6142−6147. (b) Appel, A. M.; Bercaw, J. E.; Bocarsly, A. B.; Dobbek, H.; DuBois, D. L.; Dupuis, M.; Ferry, J. G.; Fujita, E.; Hille, R.; Kenis, P. J. A.; Kerfeld, C. A.; Morris, R. H.; Peden, C. H. F.; Portis, A. R.; Ragsdale, S. W.; Rauchfuss, T. B.; Reek, J. N. H.; Seefeldt, L. C.; Thauer, R. K.; Waldrop, G. L. *Chem. Rev.* **2013**, *113*, 6621−6658. (c) Paven, M.; Papadopoulos, P.; Schottler, S.; Deng, X.; Mailander, V.; Vollmer, D.; Butt, H. J. *Nat. Commun.* **2013**, *4*, 2512. (d) Honda, M.; Tamura, M.; Nakao, K.; Suzuki, K.; Nakagawa, Y.; Tomishige, K. *ACS Catal.* **2014**, *4*, 1893−1896.

(2) (a) Takeda, Y.; Kawai, H.; Minakata, S. *Chem.—Eur. J.* **2013**, *19*, 13479−13483. (b) Ueno, A.; Kayaki, Y.; Ikariya, T. *Green Chem.* **2013**, *15*, 425−430. (c) Seayad, J.; Seayad, A. M.; Ng, J. K. P.; Chai, C. L. L. *ChemCatChem* **2012**, *4*, 774−777. (d) Jiang, H. F.; Ye, J. W.; Qi, C. R.; Huang, L. B. *Tetrahedron Lett.* **2010**, *51*, 928−932. (e) Mikkelsen, M.; Jørgensen, M.; Krebs, F. C. *Energy Environ. Sci.* **2010**, *3*, 43−81.

(3) (a) Kathalikkattil, A. C.; Tharun, J.; Roshan, R.; Soek, H. G.; Park, D. W. *Appl. Catal., A* **2012**, *447*−*448*, 107−114. (b) Wu, Y.; He, L. N.; Du, Y.; Wang, J. Q.; Miao, C. X.; Li, W. *Tetrahedron* **2009**, *65*, 6204−6210. (c) Du, Y.; Wu, Y.; Liu, A. H.; He, L. N. *J. Org. Chem.* **2008**, *73*, 4709−4712.

(4) (a) Doherty, C. M.; Buso, D.; Hill, A. J.; Furukawa, S.; Kitagawa, S.; Falcaro, P. *Acc. Chem. Res.* **2014**, *47*, 396−405. (b) Diaz, U.; Brunel, D.; Corma, A. *Chem. Soc. Rev.* **2014**, *42*, 4083−4097. (c) Zhang, F.; Jiang, H. Y.; Li, X. Y.; Wu, X. T.; Li, H. X. *ACS Catal.* **2014**, *4*, 394−401. (d) Shylesh, S.; Wagener, A.; Seifert, A.; Ernst, S.; Thiel, W. R. *Angew. Chem.* **2010**, *122*, 188−191; *Angew. Chem., Int. Ed.* **2010**, *49*, 184−187. (e) Shiju, N. R.; Alberts, A. H.; Khalid, S.; Brown, D. R.; Rothenberg, G. *Angew. Chem.* **2011**, *123*, 9789−9793; *Angew. Chem., Int. Ed.* **2011**, *50*, 9615−9619. (f) Sasidharan, M.; Fujita, S.; Ohashi, M.; Goto, Y.; Nakashima, K.; Inagaki, S. *Chem. Commun.* **2011**, *47*, 10422−10424.

(5) (a) Helms, B.; Guillaudeu, S. J.; Xie, Y.; McMurdo, M.; Hawker, C. J.; Frechet, J. M. J. *Angew. Chem.* **2005**, *117*, 6542−6545; *Angew. Chem., Int. Ed.* **2005**, *44*, 6384−6387. (b) Motokura, K.; Fujita, N.; Mori, K.; Mizugaki, T.; Ebitani, K.; Kaneda, K. *J. Am. Chem. Soc.* **2005**,

127, 9674−9675. (c) Li, P.; Cao, C. Y.; Chen, Z.; Liu, H.; Yu, Y.; Song, W. G. *Chem. Commun.* **2012**, *48*, 10541−10543. (d) Yang, Y.; Liu, X.; Li, X.; Zhao, J.; Bai, S.; Liu, J.; Yang, Q. *Angew. Chem.* **2012**, *124*, 9298−9302; *Angew. Chem., Int. Ed.* **2012**, *51*, 9164−9168. (e) Huang, Y.; Xu, S.; Lin, V. S. Y. *Angew. Chem.* **2011**, *123*, 687−690; *Angew. Chem., Int. Ed.* **2011**, *50*, 661−664.

(6) (a) Kimura, T. *J. Nanosci. Nanotechnol.* **2013**, *13*, 2461−2470. (b) Ma, T. Y.; Yuan, Z. Y. *ChemSusChem* **2011**, *4*, 1407−1419. (c) Ma, T. Y.; Li, H.; Tang, A. N.; Yuan, Z. Y. *Small* **2011**, *7*, 1827−1837. (d) Zhu, Y. P.; Ma, T. Y.; Liu, Y. L.; Ren, T. Z.; Yuan, Z. Y. *Inorg. Chem. Front.* **2014**, *1*, 360−383. (e) Ma, T. Y.; Lin, X. Z.; Yuan, Z. Y. *Chem.—Eur. J.* **2010**, *16*, 8487−8494. (f) Ma, T. Y.; Lin, X. Z.; Yuan, Z. Y. *J. Mater. Chem.* **2010**, *20*, 7406−7415. (g) Dutta, A.; Pramanik, M.; Patra, A. K.; Nandi, M.; Uyama, H.; Bhaumik, A. *Chem. Commun.* **2012**, *48*, 6738−6740.

(7) (a) Ma, T. Y.; Liu, L.; Deng, Q. F.; Lin, X. Z.; Yuan, Z. Y. *Chem. Commun.* **2011**, *47*, 6015−6017. (b) Ma, T. Y.; Yuan, Z. Y. *Chem. Commun.* **2010**, *46*, 2325−2327. (c) Jones, D. J.; Aptel, G.; Brandhorst, M.; Jacquin, M.; Jiménez-Jiménez, J.; Jiménez-López, A.; Maireles-Torres, P.; Piwonski, I.; Rodrígues-Castellón, E.; Zajac, J.; Rozière, J. *J. Mater. Chem.* **2000**, *10*, 1957−1963. (d) Bhaumik, A.; Inagaki, S. *J. Am. Chem. Soc.* **2001**, *123*, 691−696.

(8) Conley, M. P.; Coperet, C.; Thieuleux, C. *ACS Catal.* **2014**, *4*, 1458−1469.

(9) Liu, B.; Tu, M.; Zacher, D.; Fischer, R. A. *Adv. Funct. Mater.* **2013**, *23*, 3790−3798.

(10) Naumkin, A. V.; Kraut-Vass, A.; Gaarenstroom, S. W.; Powell, C. J. *NIST-X-ray Photoelectron Spectroscopy Database 20*, version 4.1; National Institute of Standards and Technology: Gaithersburg, MD, 2012.

(11) (a) Gagnon, K. J.; Perry, H. P.; Clearfield, A. *Chem. Rev.* **2012**, *112*, 1034−1054. (b) Shimizu, G. K. H.; Vaidhyanathan, R.; Taylor, J. M. *Chem. Soc. Rev.* **2009**, *38*, 1430−1449.

(12) An, K.; Alayoglu, S.; Musselwhite, N.; Na, K.; Somorjai, G. A. *J. Am. Chem. Soc.* **2014**, *136*, 6830−6833.

(13) (a) Darensbourg, D. J.; Chung, W. C.; Wang, K. C.; Zhou, H. C. *ACS Catal.* **2014**, *4*, 1511−1515. (b) Li, J. R.; Yu, J.; Lu, W.; Sun, L. B.; Sculley, J.; Balbuena, P. B.; Zhou, H. C. *Nat. Commun.* **2013**, *4*, 1538.

(14) (a) An, J.; Geib, S. J.; Rosi, N. L. *J. Am. Chem. Soc.* **2010**, *132*, 38−39. (b) Couck, S.; Denayer, J. F. M.; Baron, G. V.; Rémy, T.; Gascon, J.; Kapteijn, F. *J. Am. Chem. Soc.* **2009**, *131*, 6326−6327. (c) Ide, Y.; Kagawa, N.; Sadakane, M.; Sano, T. *Chem. Commun.* **2013**, *49*, 9027−9029. (d) Hao, S.; Chang, H.; Xiao, Q.; Zhong, Y.; Zhu, W. *J. Phys. Chem. C* **2011**, *115*, 12873−12882.

(15) (a) Sayari, A.; Belmabkhout, Y. *J. Am. Chem. Soc.* **2010**, *132*, 6312−6314. (b) Caplow, M. *J. Am. Chem. Soc.* **1968**, *90*, 6795−6803.

(16) (a) Colombo, V.; Montoro, C.; Maspero, A.; Palmisano, G.; Masciocchi, N.; Galli, S.; Barea, E.; Navarro, J. A. R. *J. Am. Chem. Soc.* **2012**, *134*, 12830−12843. (b) Yue, M. B.; Sun, L. B.; Cao, Y.; Wang, Z. J.; Wang, Y.; Yu, Q.; Zhu, J. H. *Microporous Mesoporous Mater.* **2008**, *114*, 74−81.

(17) Luo, Y. R. *Handbook of Bond Dissociation Energies in Organic Compounds*; CRC Press: Boca Raton, FL, 2002.

(18) (a) Cho, H. J.; Dornath, P.; Fan, W. *ACS Catal.* **2014**, *4*, 2029−2037. (b) Gu, D.; Schüth, F. *Chem. Soc. Rev.* **2014**, *43*, 313−344.